Estuaries and Coasts
DOI 10.1007/s12237-016-0076-2

Reconstruction of Recent Sedimentary Processes in a Carbonate Platform (Gulf of Batabano, Cuba) Using Environmental Radiotracers

M. Díaz-Asencio [1,4] · J. A. Corcho-Alvarado [2,3] · J. A. Sánchez-Cabeza [4] · A. C. Ruiz-Fernández [4] · M. Eriksson [5]

Received: 22 June 2015 / Revised: 6 January 2016 / Accepted: 1 February 2016

Abstract Recent (past 100 years) sedimentary processes in the highly dynamic Gulf of Batabano (Cuba, Caribbean Sea) were investigated through the analyses of environmental radionuclides (e.g., ^{210}Pb, ^{226}Ra, ^{137}Cs, ^{239,240}Pu, and ^{14}C) in nine sediment cores. We evaluated the mean mass accumulation rates (MARs) and the surface mixed layers (SMLs) in each sediment core. Based on these results, three sedimentary environments were identified in the study region. In the central zone, the sediments were mainly composed of carbonate transported from the southern area and showed elevated mass accumulation rates (MAR, 0.11–0.23 g cm^{-2} year^{-1}) and relatively deep surface mixed layers (SML, 14–16 cm). The southwestern zone was characterized by lower MAR (0.05–0.08 g cm^{-2} year^{-1}) and thinner SML (7–8 cm). In both areas, the long sediment mixing times in the SMLs (of 45–61 years) smoothed out the sedimentary records. The coastline sedimentary environments were characterized by higher MAR (0.30–0.57 g cm^{-2} year^{-1}) and the sedimentary records displayed clear signatures of extreme climatic events such as the intensive rains in 1999 reported for La Coloma and the hurricanes Lili and Isodore in 2002. Our study shows that the application of the ^{210}Pb sediment dating method in dynamic costal zones is a challenging task but still may provide important information regarding sedimentation and mixing processes in the ecosystem.

Keywords Gulf of Batabano · Lead-210 · Sediment geochronology · Recent sedimentation · Carbonate platform

Communicated by Marco Bartoli

Highlights
1. Dating of recent sediments in highly dynamic coastal marine ecosystem
2. Use of ^{210}Pb (^{226}Ra), ^{239,240}Pu, and ^{14}C for dating coastal marine sediments
3. Sedimentation and mixing processes over the past 100 years in coastal marine sediments
4. Impact of climatic events (hurricanes, rains) on sedimentation process in coastal environments

✉ M. Díaz-Asencio
misaeldiazasencio1971@gmail.com; misael@ceac.cu

[1] Centro de Estudios Ambientales de Cienfuegos, CITMA-Cienfuegos, Cienfuegos, Cuba

[2] Institute of Radiation Physics, Lausanne University Hospital, Rue du Grand-Pré 1, 1007 Lausanne, Switzerland

[3] SPIEZ LABORATORY, Federal Office for Civil Protection, 3700 Spiez, Switzerland

[4] Instituto de Ciencias del Mar y Limnología, Universidad Nacional Autónoma de México, 4510 Ciudad de México, México

[5] Marine Environment Laboratories, IAEA, Quai Antoine 1er, Monaco

Introduction

Sediments in coastal areas can be regarded as reliable archives of past environmental processes and can be used to obtain information about changes in fluxes of nutrients and pollutants and in recent sedimentation processes (Santschi et al. 2001; Díaz-Asencio et al. 2009). The most widely used method to estimate recent (<100 years) sedimentation rates is by means of the naturally occurring radioisotope ^{210}Pb, which has a half-life of 22.3 years (Appleby and Olfield 1978; Sanchez-Cabeza and Ruiz-Fernández 2012). ^{210}Pb, a radionuclide from the natural ^{238}U decay series, is mainly introduced to the coastal zone by atmospheric deposition. The ^{210}Pb dating method is commonly corroborated by comparison with the time-dependent deposition of the anthropogenic fallout radionuclides ^{137}Cs and ^{239,240}Pu (e.g.,

Published online: 09 February 2016

Robbins and Edgington 1975; Sanchez-Cabeza et al. 1999; Díaz-Asencio et al. 2011).

Best results using the ^{210}Pb method are normally obtained in low dynamic environments in which steady state conditions are assumed. In dynamic systems, such as marine coastal areas, numerous studies have shown that processes other than sedimentation affect the distribution of ^{210}Pb in the sediments. The most important process influencing the distribution is particle mixing (Carpenter et al. 1982; Boer et al. 2006; Smoak 2015). The application of the ^{210}Pb dating methods in highly dynamic areas is therefore a challenging task and the results may entail large uncertainties due to sediment mixing. Nonetheless, this sediment dating method remains the most used dating approach to gain information about sedimentation and mixing processes in dynamic systems (Rude and Aller 1991; Henderson et al. 1999; Robbins et al. 2000; Boer et al. 2006).

The Gulf of Batabano is one of the most important coastal resources of the Cuban archipelago. Notably, this ecosystem provides about 60 % of the total lobster catch on the Cuban shelf (Baisre 2010). However, since 1990, the lobster catch in this region has consistently declined. Biological studies have evidenced signs of strong environmental degradation in the gulf such as loss of biodiversity, shift of benthic communities (Cerdeira-Estrada et al. 2008) and reduction in size and capture levels of commercially valuable species (Puga et al. 1996; Caddy and Agnew 2004). Potential factors causing this degradation include (i) deterioration/loss of habitats, (ii) malpractice of fisheries management, and (iii) decrease in primary productivity (Cruz et al. 2001; Puga et al. 2005; González-Yáñez et al. 2006; Claro et al. 2009). However, the scarce information available from the Gulf of Batabano hinders a better identification of the main causes of the environmental degradation.

Hence, the aim of this work is to establish the chronology of recent sedimentary processes in the shallow environments of the Gulf of Batabano. For this purpose, we use the well-established chronology methods based on the combination of natural (^{210}Pb, ^{226}Ra, ^{14}C) and anthropogenic (^{239,240}Pu and ^{241}Am) radionuclides. The simultaneous use of these methods in sediment cores from different areas of the gulf provides an understanding of sedimentation and mixing at a basin level.

Materials and Methods

Study Area

The Gulf of Batabano is a large (20 850 km^2) semienclosed water body in southwestern Cuba (Fig. 1). The gulf is a shallow (mean depth of 6 m) carbonate platform subject to terrigenous inputs due to its closeness to mainland. The coastal area is predominantly fringed by mangrove forests. Seaward boundaries (Caribbean Sea) are marked by coral reef ecosystems and the hydrodynamic regime notably increases at the shelf border. Subtidal habitats near the coast are predominantly classified as muddy with scarce vegetation (Cerdeira-Estrada et al. 2008). In the central part of the gulf, unconsolidated sediments form habitats such as bare sand, mud flats, and macroalgal beds. General water circulation is controlled by the Caribbean currents and the prevailing winds, mainly flowing in the southeast to west and southwest directions (Hernandez and Diaz 2003).

The gulf is dotted with many small islands and keys and is subject to terrigenous influence from the mainland, principally in the northwest region (Avello and Pavlidis 1986). The salinity is close to that of the open sea (i.e., 32–35 ‰), but lower in the coastal zone due to terrestrial runoff. Silt- and sand-sized sediments occur mainly in the southeast and along the southern edge of the gulf. Carbonate mud and muddy skeletal sediments are present in the central, western, and northern areas. The spatial distribution of the grain size fractions is primarily influenced by three environmental factors: hydrodynamic conditions, character of the biota, and salinity (Hoskins 1964; Avello and Pavlidis 1986).

Sampling and Sample Preparation

Our experimental approach to investigate the Gulf of Batabano is based on sampling and analyzing one sediment core per sampling site. This is a common approach for studying historical trends and regional patterns in large areas such as bays and gulfs (Robbins et al. 2000; Boer et al. 2006).

In November 2005, nine sediment cores were collected in the Gulf of Batabano (Fig. 1). The sampling sites were selected in zones undisturbed by human activities such as fishing or dredging, because these activities may eliminate or modify the environmental records stored in the sediments. A UWITEC corer with PVC liner (60 cm length, 8.6 cm inner diameter) was used to collect the sediment cores. The transparency of the water allowed scuba divers to assist ensuring minimum disturbance of the water-sediment interface as well as sampling from surfaces without vegetation and no evidence of bioturbation.

The sediment cores were collected in shallow waters with depths ranging from 3 to 12 m. The length of the collected sediment cores ranged from 28 to 52 cm. General information about the sampling sites and surface sediments are provided in Table 1. Each sediment core was sliced into 1-cm thick sections until 10-cm depth, then into 2-cm thick sections between 10 and 20-cm depth, and into 5-cm thick sections below 20 cm. Each section was freeze-dried, homogenized, and sieved through 1-mm mesh to separate sediments from other materials such as corals and mollusk shells. After sieving, both fractions were weighed and stored in plastic vials for subsequent analysis. Further treatments described below were

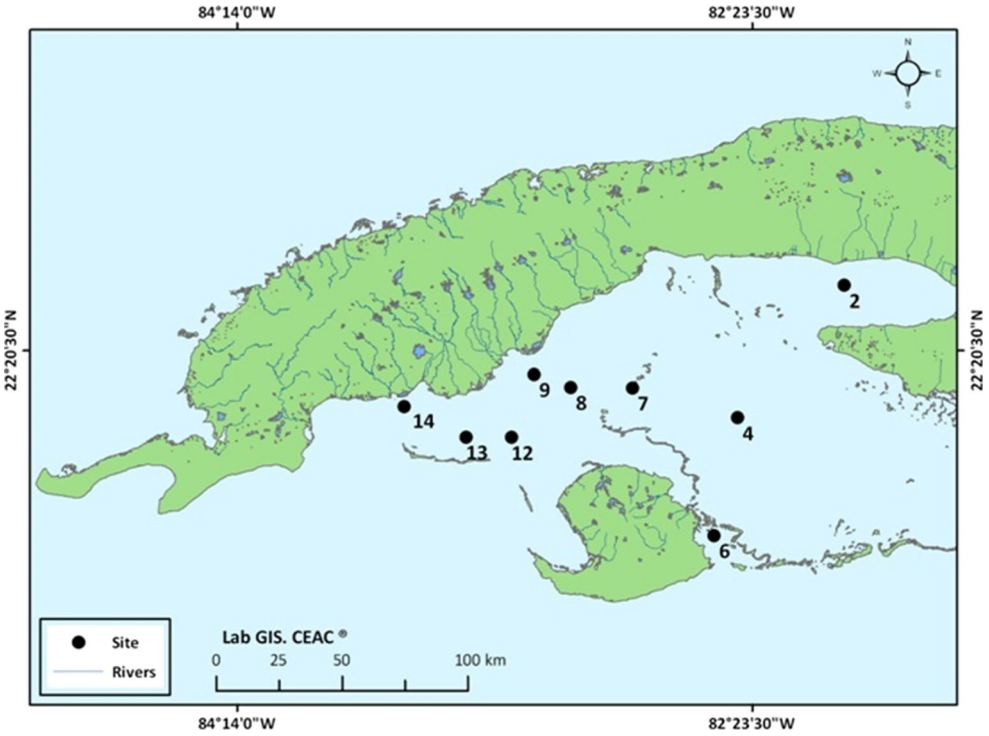

Fig. 1 Study area in the Gulf of Batabano, Caribbean Sea. Sampling sites are indicated

performed in the sediment fraction smaller than 1 mm unless otherwise declared. The dry weight of the sediment was used to determine the in situ dry bulk density and the mass accumulation depth according to Sanchez-Cabeza et al. (2012).

Grain Size Analysis

The particle size of the sediments was determined by laser dispersion with a MALVERN Mastersizer Micro v2.12. For this, 1 g of dry sediment was sieved to separate the fraction with particle sizes below 300 μm. A 0.5-g aliquot of this fraction (<300 μm) was then diluted in MilliQ water and 0.16 N NH_4OH was added as a dispersive agent. The solution was pumped and circulated through a laser beam to determine the particle size distribution.

Radionuclides

^{226}Ra and ^{137}Cs were analyzed by high-resolution gamma spectrometry using a low-background intrinsic germanium

Table 1 General information about the cores and surface sediments in the sampling stations in the Gulf of Batabano

Site	Location	Core length (cm)	Water depth (m)	S (‰)	Remarks on surface sediments	Mean grain size
2	22° 34.390 N 82° 03.420 W	30	7	28	Silty No vegetation, small hole was observed	Silty sand
4	22° 06.000 N 82° 25.980 W	44	5	34	Sandy, white sediments, scarce seagrass vegetation	Sand-silty sand
6	21° 41.420 N 82° 28.305 W	42	3	34	Close to mangroves Sulfide smell	Sand-silty sand
7	22° 12.450 N 82° 48.646 W	48	5	35	Sandy, white sediment	Sand-silty sand
8	22° 11.969 N 83° 01.806 W	52	7	34	Sandy, white sediment, scarce seagrass vegetation	Silty sand
9	22° 15.299 N 83° 10.134 W	43	8	34	Silty Scarce vegetation	Sand-silty sand
12	22° 04.593 N 83° 24.023 W	46	12	34	Silty no vegetation Sulfide smell	Silty sand-sand
13	22° 06.530 N 83° 35.760 W	45	8	33	Silty no vegetation Sulfide smell	Sand
14	22° 09.360 N 83° 40.390 W	45	6	33	Silty no vegetation Sulfide smell	Sand

well detector (CAMBERRA, model EGPC100P15, with an energy resolution of 2.1 keV at 1333 keV). Approximately 6 g of dry sediments were placed in sealed plastic containers and stored for at least 3 weeks in order to allow ^{226}Ra to reach equilibrium with its daughter nuclides. ^{226}Ra was determined via the 352-keV gamma rays emitted by its daughter nuclide ^{214}Pb and ^{137}Cs was determined through its gamma line at 662 keV. Efficiency calibration was performed using both a Standard Uranium Ore (IAEA-RGU-1) and a Certificated Reference Solution QCY44 (Amersham). Replicate analyses of the certified reference materials IAEA-313 (Stream sediment), IAEA-385 (Irish Sea sediment), and IAEA-384 (Fangataufa sediment) provided consistent results within 1σ uncertainty of the reported activities of ^{226}Ra and ^{137}Cs.

Total ^{210}Pb activity was determined by high-resolution α spectrometry of its decay product ^{210}Po, assuming secular equilibrium between both radionuclides. Aliquots of dry sediment (ca. 0.5 g) were spiked with ^{209}Po as a yield tracer and dissolved by microwave digestion in a mixture of 1:1:0.5 HNO_3/HCl/HF (Sanchez-Cabeza et al. 1998). ^{210}Po was deposited spontaneously onto silver discs and counted in a Canberra integrated alpha spectrometer with PIPS detectors (active area of 450 mm^2; 18 keV of nominal resolution). The IAEA-384 reference material (certified value for ^{210}Po 22 [21–23] Bq kg^{-1}) was used for data quality control with excellent results in all the analyses (20.5 ± 1.0 Bq kg^{-1}, n = 18).

Supported ^{210}Pb ($^{210}Pb_{sup}$) in each layer was derived from the ^{226}Ra activity obtained by gamma spectrometry. ^{210}Pb in excess ($^{210}Pb_{ex}$) in each section was calculated from the difference between total and supported ^{210}Pb ($^{210}Pb_{ex} = {}^{210}Pb - {}^{210}Pb_{sup}$).

Previous studies in coastal sediments have demonstrated that ^{239,240}Pu is an excellent alternative to ^{137}Cs as a chronostratigraphic marker (Díaz-Asencio et al. 2011; Corcho-Alvarado et al. 2014; Sanders et al. 2014). ^{239,240}Pu and ^{241}Am measurements were used to corroborate the ^{210}Pb sediment chronologies in cores 9 and 14, collected in different sedimentary environments.

The ^{239,240}Pu and ^{241}Am analyses were performed on the fine sediment fraction (<63 μm) in order to increase sensitivity. Approximately 10 g of dry sediment was diluted in MilliQ water and 0.16 N NH_4OH, and the solution was sieved through a 63-μm mesh to remove small amount of shell fragments, roots, and other plant matter (Baskaran and Naidu 1995; Robbins et al. 2000). The sediments were dried and ashed at 550 °C for 48 h prior to the analyses. The radiochemical method combines high pressure microwave digestion in 8 M HNO_3 for the dissolution of the sample and the highly selective extraction chromatographic resins TEVA and DGA (Triskem International, Bruz, France) for the separation and purification of Pu and Am (Luisier et al. 2009). The alpha sources were prepared by electrodeposition onto stainless steel discs, and then measured by high-resolution alpha spectrometry with PIPS detectors (Alpha Analyst, Canberra Electronic).

In order to determine the age of the two bottom sections (37.5 and 45 cm depth) of the sediment core 7, radiocarbon measurements were performed in the shell fragments (Fig. 1). The shells were extracted from the freeze-dried sediment (before sieving) using stainless steel tweezers. The radiocarbon measurements were performed at the National Ocean Sciences AMS Facility (Woods Hole Oceanographic Institution, USA). The radiocarbon ages were calibrated with INTCAL09 (Reimer et al. 2009).

Organic and Inorganic Carbon

The content of total carbon was measured using a CHN analyzer (Carlo Erba model 1602). Approximately 100–150 mg of dry sediment was encapsulated into a Sn foil cup and introduced into a combustion furnace. Organic carbon was determined after treating the samples with concentrated HCl to remove inorganic carbon. Concentration is expressed as the percentage of total dry weight. The reference materials Soil 502–062 Batch 1012 and Soil 502–309 Batch 1012 were used for quality control purposes.

Major and Trace Elements

Major elements (Al, Si, Ca, Fe) were measured by energy dispersion X-ray fluorescence (XRF) spectrometry using a SPECTROR X-LAB PRO 2000 system. The equipment was calibrated for 4-g samples in sample cups covered with 4-μm thick Prolene® thin film. Cups were filled with 4 g of dry and sieved (1-mm mesh size) sediment. The XRF analysis was performed by combining measurements with three different targets and enabled the determination of elements from atomic number 13 (Al) to 92 (U). The reference materials IAEA-405 and IAEA-433 were used for quality control purposes and results obtained fell within the reported interval of certified values.

Mercury

Samples were sieved through a 63-μm plastic mesh and 20–50-mg aliquots were placed in precleaned combustion containers. Total mercury concentrations were determined by using an Advanced Mercury Analyser (LECO AMA-254) with detection limit of 0.01 ng Hg (method 7473, US EPA). We used the reference solutions FISHER SM114-100 with concentrations ranging from 0 to 600 ng of total Hg for calibration. Analytical quality was assessed by analyzing replicate samples and standard reference materials NIST 2709 and BCR 146; results obtained fell within the reported certified values.

^{210}Pb age Dating

The mean mass accumulation rate (MAR) was determined through the constant flux/constant sedimentation (CFCS) dating model which assumes a constant flux of ^{210}Pb and a constant mean MAR within the period analyzed (see, for example Robbins and Edgington 1975; Sanchez-Cabeza and Ruiz-Fernández 2012). The effect of mixing was taken into account by applying the CFCS model to the $^{210}Pb_{xs}$ profile beneath the surface mixed layer (SML), under the assumption that homogeneous mixing occurs in the SML and that it has a constant thickness with time (Nittrouer et al. 1984; Lewis et al. 2002; Boer et al. 2006). In these cases, using the CFCS model with constant SML allowed determination of the mean MAR (in the burial region) and to estimate the time represented by the SML. In this model, the age assigned to each section has an uncertainty equivalent to the SML expressed in time units. Hence, the increase of the SML compromises the time resolution of the sedimentary records. We applied this model to interpret the sedimentation process in cores 2, 4, 6, 7, 8, 9, 12, and 13.

Non-monotonically variations of $^{210}Pb_{ex}$ cannot be interpreted with the CFCS model. In such cases, the constant flux (CF) model (Sanchez-Cabeza and Ruiz-Fernández 2012; also known as CRS, Appleby and Oldfield 1978) is more appropriate. The CF model assumes a constant $^{210}Pb_{ex}$ flux to the sediment surface, so MAR may change over time. This model can be used in most sedimentary systems where the sediment supply may vary in response to climatic or anthropogenic changes. We applied the CF model to the core 14 to calculate the MAR and the date of sedimentation for each section. Oldfield and Appleby (1984) pointed out that there is no significant difference between CRS model-derived results assuming no mixing and those determined assuming mixing, when the thickness of the mixing layer does not exceed 15 % of the total thickness of the $^{210}Pb_{ex}$ profile. Irrespective of the shape of the $^{210}Pb_{ex}$ activities profile, these data can be integrated to estimate the $^{210}Pb_{ex}$ inventory (Bq m^{-2}) from which the $^{210}Pb_{ex}$ flux (Bq m^{-2} year^{-1}) can be calculated (Sanchez-Cabeza and Ruiz-Fernández 2012). The ^{210}Pb flux was calculated in all cores. In core 2, where the $^{210}Pb_{ex}$ inventory is incomplete ($^{210}Pb_{ex}$ does not reach the zero value), it was necessary to estimate the missing inventory in order to calculate the ^{210}Pb flux (Appleby and Olfield 1978).

In core 14, characterized by conspicuous changes in the grain size distribution and other major and trace elements, the $^{210}Pb_{ex}$ profile was normalized by Al in order to verify that such anomalies of the $^{210}Pb_{ex}$ profile were caused by changes in sediment composition (Ruiz-Fernández et al. 2009):

$$^{210}Pb_{ex}* = {}^{^{210}Pb_{ex}}/_{F_n}; \quad F_n = {}^{Al_i}/_{Al_{bkg}}$$

where F_n is the ratio of Al_i (Al concentration at each layer of the core) to Al_{bkg} (Al concentration at the bottom part of the core).

The total ^{239,240}Pu inventories were calculated by summing the product of each section's activity, thickness, and sediment bulk density. For the missing ^{239,240}Pu data, the activity was estimated by interpolating the activities of two neighbor layers. In the case of core 9, a constant activity of ^{239,240}Pu was assumed within the SML.

Results

Sediment Characteristics

During the sampling period, the salinity was fairly constant at all sites (32–33 ‰), except station 2 (28 ‰). In core 2, we observed evidence of a benthic worm in the surface. The color of the sediments changed significantly in certain cores, especially at the bottom of cores 4, 6, 7, and 8 (the color changed from white to dark brown).

In sediment cores 4, 7, 8, 9, 12, and 13, the content of particles with sizes <300 μm was between 51 and 77 %; and the distribution profile showed slight variations down core, with a maximum of 15 % (Fig. 2). In cores 2 and 6, the downcore variability was larger, with values up to 26 %. A slight increase of the fine fraction (<300 μm) was observed in the top layers of the sediment cores 2, 8, 12, and 13.

Natural and Anthropogenic Radionuclides in the Sediments

^{210}Pb was found in the upper 45 cm of all cores with activities below 60 Bq kg^{-1} (Fig. 3). The highest ^{210}Pb activities were found in the surface layers (0–5 cm) of cores 2, 6, and 14; whereas the lowest ^{210}Pb activities were found in the surface layers (0–3 cm) of cores 4 and 7. The activities of ^{226}Ra were rather similar in most of the sediment cores (cores 2, 9, 12, 13, 14), with mean values ranging from 9 to 13 Bq kg^{-1} (Fig. 3). The lowest ^{226}Ra activities (<5 Bq kg^{-1}) were observed in the central part of the gulf (cores 4, 7, and 8), and the highest activities were found in the bottom layers of cores 6 and 7. The ^{210}Pb activity at 40–43-cm depth in core 7 was 60 Bq kg^{-1}, which is approximately three times higher than near surface ^{210}Pb activity. Secular equilibrium between ^{226}Ra and ^{210}Pb was reached in all cores, except core 2. The constant activity of ^{210}Pb in the surface layer of cores 2, 4, 6, 7, 8, 9, 12, and 13 indicates the existence of a strong mixing, which is consistent with approximately constant grain size distribution at the surface layer in cores 4, 6, 7, 8, 9, and 12 (Fig. 2).

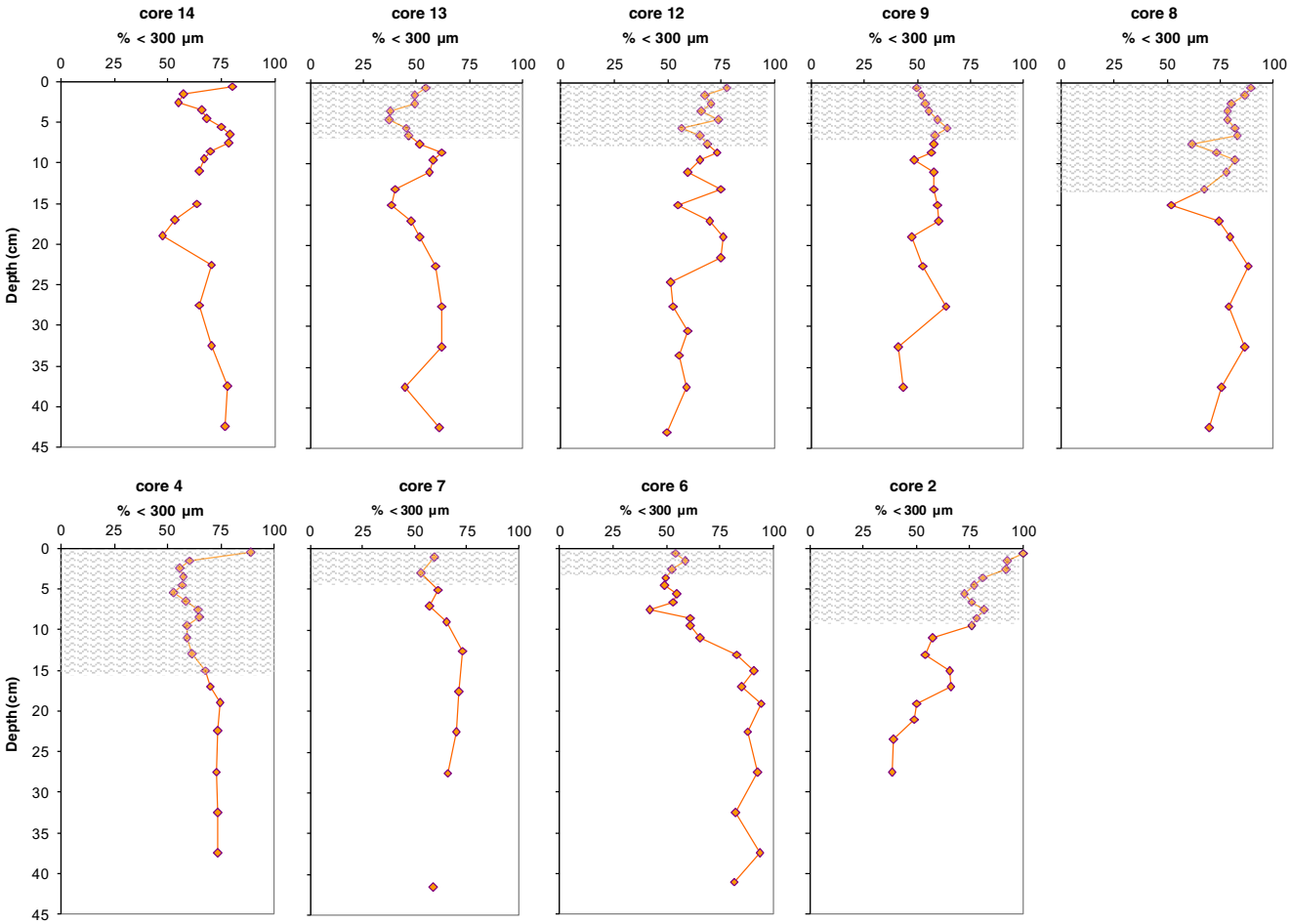

Fig. 2 Vertical distribution of the fraction of particles with size below 300 μm in all sediment cores. The SML in each core is shown

The activity of ^{137}Cs was above the detection limit (0.7 Bq kg^{-1}) only in the cores 2 and 14 (Fig. 4). ^{239,240}Pu and ^{241}Am were measured in sediment cores 9 and 14. Core 9 was collected at 10 km from the coastal area (Fig. 1) and characterized by a large SML with nearly constant ^{210}Pb (Fig. 3). ^{239,240}Pu activities within the SML were also nearly constant (Fig. 4b). Below the SML, ^{239,240}Pu activities steadily decreased and approached the detection limit at 20–25-cm depth.

Core 14 was collected near the coastal line (Fig. 1) and does not show an SML (Fig. 3). ^{239,240}Pu activities in this core were slightly higher than in core 9 (Fig. 4c). The changes in grain size distribution in core 14 are also reflected in some abnormalities of the artificial radionuclide profiles. The ^{239,240}Pu and ^{241}Am depth profiles seem to be more impacted by the changes in the particle size distribution than that of ^{137}Cs (Fig. 4c). Higher activities of these radiotracers are mostly associated with smaller particle sizes. The ^{239,240}Pu (and ^{241}Am) depth profile shows two broad peaks at 6 and at 22–23-cm depth, and nearly constant activities between both peaks. At depths below 30 cm, their activities are below the limits of detection.

Geochronology With ^{210}Pb and Anthropogenic Radionuclides

The ^{210}Pb$_{ex}$ depth profiles in the cores are shown (Fig. 5) and the main results of the CFCS dating model are reported in Table 2. In all the cores, ^{210}Pb$_{ex}$ shows a decreasing trend with depth beneath the SML. Most cores (except 2 and 7) show an intermediate transitional layer between the zones of burial of sediments (only sedimentation) and the SML. The highest mean MAR of 0.57 g cm^{-2} year^{-1} was calculated in core 2. For the rest of the cores, the mean MAR varies from 0.04 to 0.23 g cm^{-2} year^{-1}. The thickness of the SML in the cores, expressed in time units (SML in mass depth per mean MAR), ranges from 17 to 65 years (Table 2).

The ^{210}Pb$_{ex}$ profile in core 14 did not show an SML or the typical exponential decrease (Fig. 6a). This core was characterized by conspicuous changes in the grain size distribution (Fig. 6b) and in the concentrations of Al and organic carbon (Fig. 6c, d). The ^{210}Pb$_{ex}$ profile was normalized by the Al concentration.

The normalized ^{210}Pb$_{ex}$ depth profiles did show a lower variability in comparison with the original ^{210}Pb$_{ex}$ profile

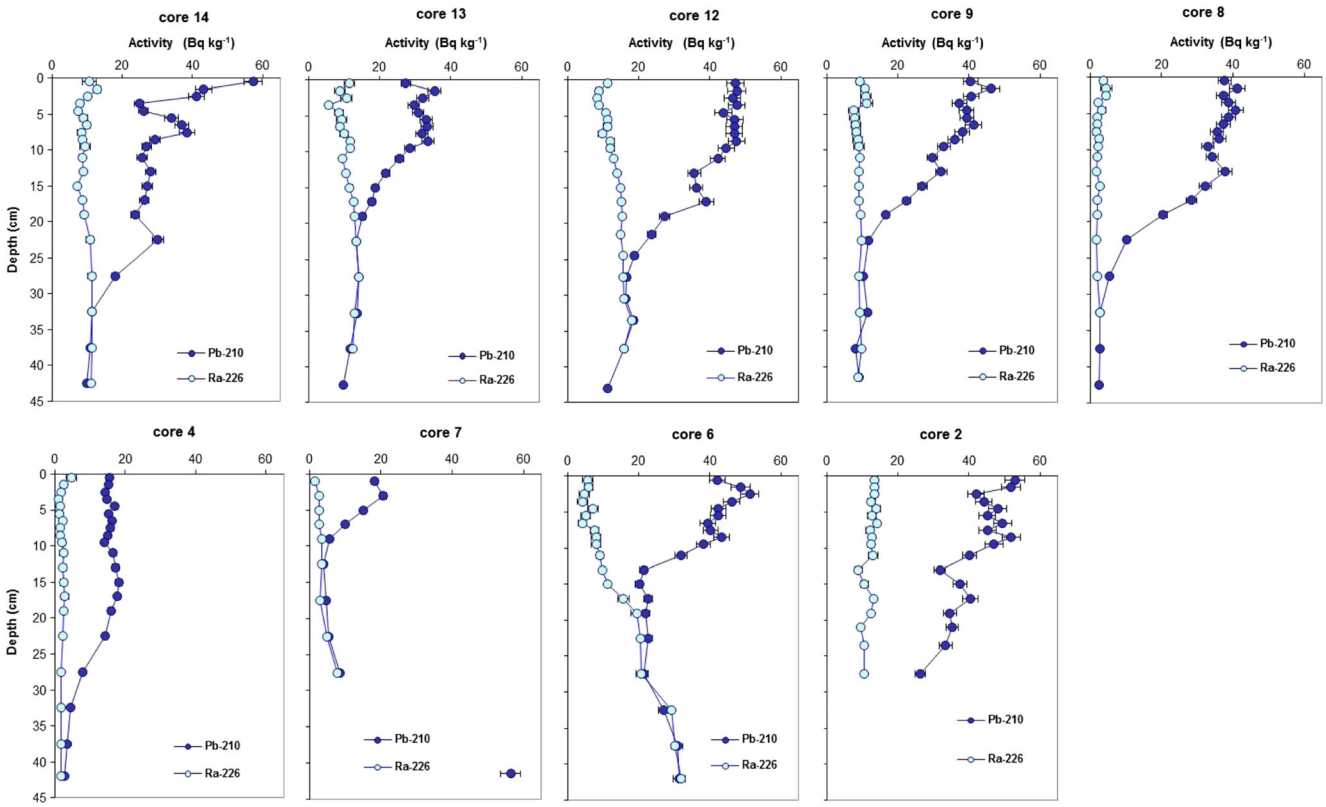

Fig. 3 Activity-depth profiles of ^{210}Pb, ^{226}Ra, and ^{137}Cs in nine cores of Gulf of Batabano. ^{137}Cs was detected only in cores 2 and 14

(Fig. 6). The CFCS dating model was then used to interpret both the original and the normalized profiles. The derived MARs using normalized and raw $^{210}Pb_{ex}$ data were comparable within their uncertainties (0.42 ± 0.09 and 0.30 ± 0.03 g cm^{-2} year^{-1}). The significant correlation ($R^2 = 0.85$, $P < 0.05$) and the lower uncertainty of the MAR indicates that the CFCS model better describes the normalized $^{210}Pb_{ex}$ profile (Fig. 6f). The CF model was used as well to interpret the $^{210}Pb_{ex}$ profile in core 14. The MARs in core 14, calculated with the CF model, showed increasing values after 1970, with a peak around 1993 and 2002 (Fig. 7). The CF MARs were comparable to

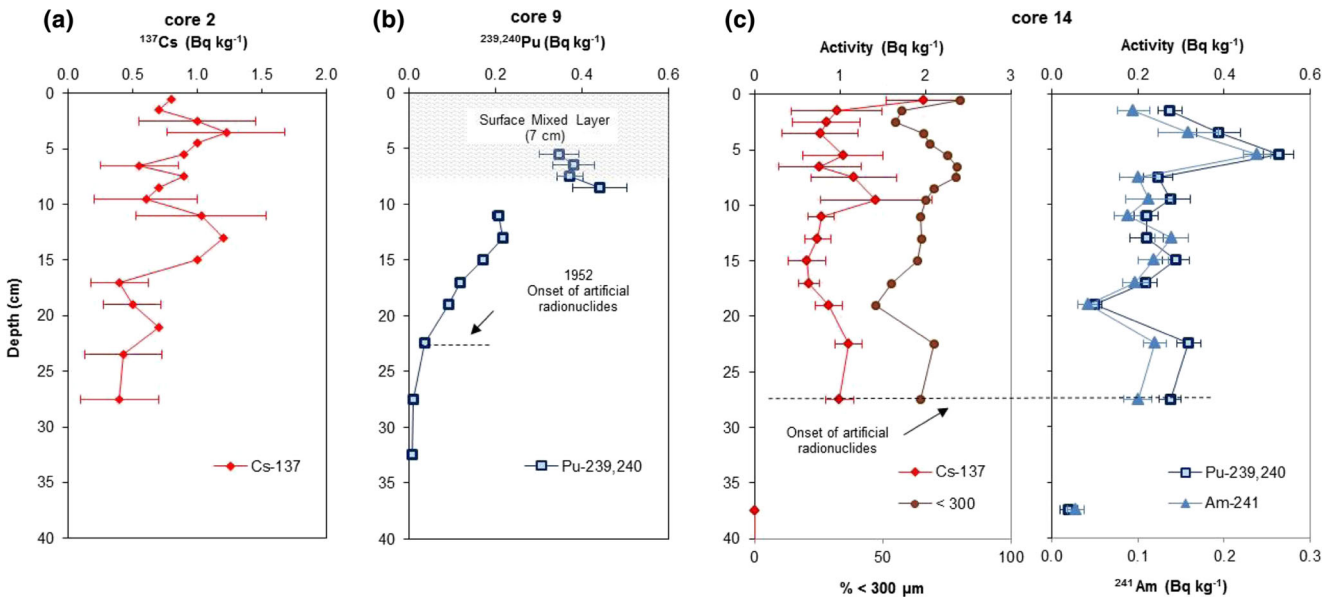

Fig. 4 **a** ^{137}Cs profile in core 2. **b** ^{239,240}Pu depth profile in core 9. **c** Depth profiles of ^{239,240}Pu, ^{241}Am, and ^{137}Cs activities in core 14. The depths of the fallout onset are also given

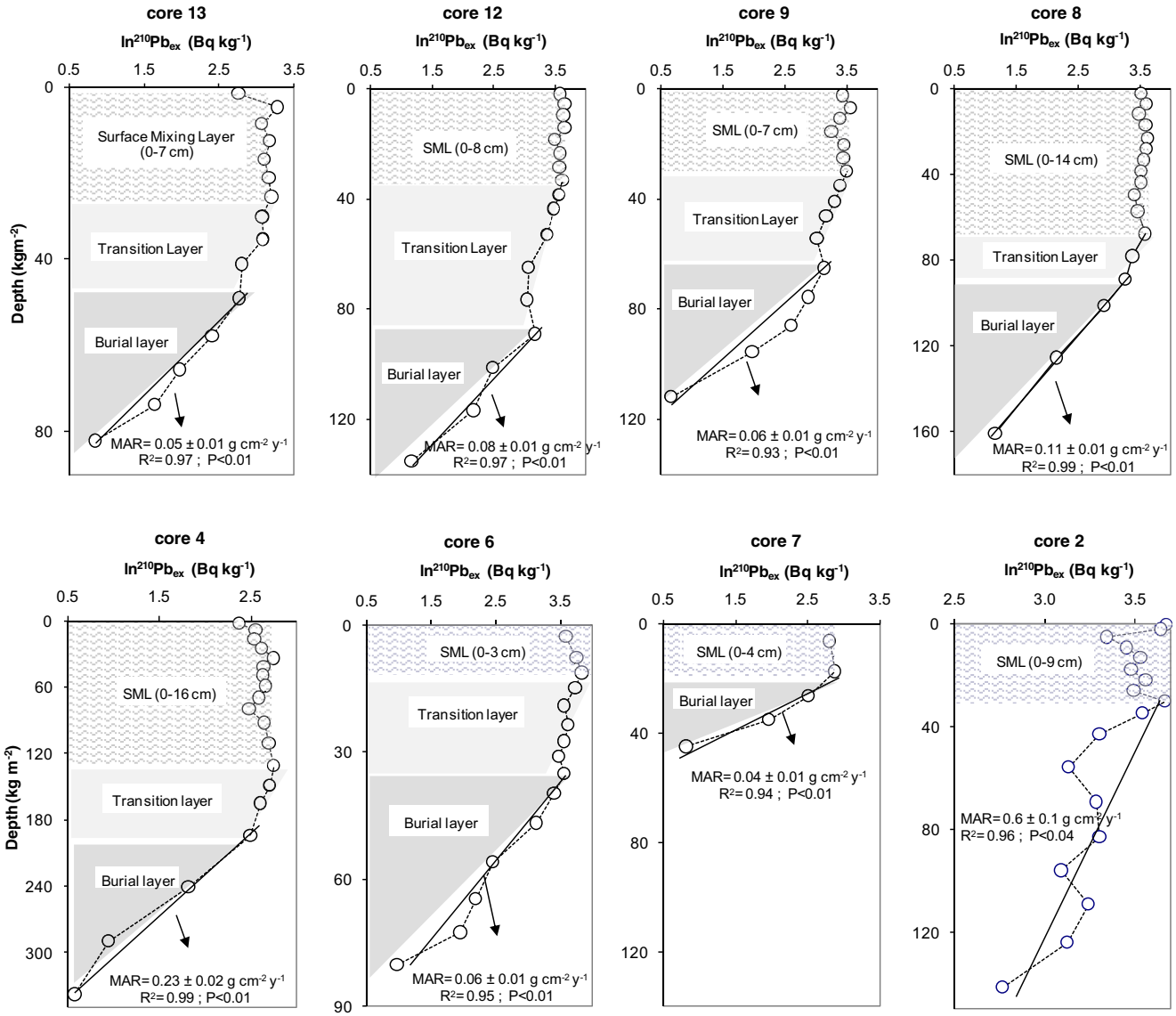

Fig. 5 Vertical profiles of $^{210}Pb_{ex}$ for the nine cores of the Gulf of Batabano. The mean MAR calculated using the CFCS model in the burial layer (below the SML and transition layer) are also shown

the mean MAR calculated with the CFCS model using the normalized $^{210}Pb_{ex}$ profile after 1970 (Fig. 6f).

The use of ^{137}Cs as a chronostratigraphic tracer in the Batabano Gulf is limited by the extremely low levels of this radionuclide in the sediment samples. Moreover, due to the large uncertainties of the ^{137}Cs data in core 14, we cannot distinguish any variability of this radionuclide in the depth sections from 1 to 12 cm (Fig. 4c). The $^{239,240}Pu$ (and ^{241}Am in core 14) profiles in sediment cores 9 and 14 did not show well-developed peaks corresponding to the expected radionuclide fallout maximum in 1963 (Fig. 4b, c). In core 9, $^{239,240}Pu$ activities were below the detection limits at depths greater than 25 cm (Fig. 4b). In core 14, $^{239,240}Pu$ activities were below the detection limits at depths greater than 30 cm, the layer 25–30 cm is taken then as the layer containing the onset fallout of $^{239,240}Pu$ and ^{241}Am (Fig. 4c).

Discussion

Sediment Chronologies

In cores 9, 12, and 13, the SML was 7 to 8 cm thick. A larger SML of 16 cm was observed in core 4. Core 4 was collected in the central part of the gulf (Fig. 1), an area known to be highly affected by sea currents and winds, which are the principal cause of water column mixing and resuspension of settled material in the gulf (Hernández and Díaz, 2003; Alonso-Hernández et al. 2011). A thinner SML of 3 cm was observed in core 6. This core was collected in an area which is surrounded by a barrier of small islands and vegetation and is therefore protected from sea currents and winds. The large SML of 9 cm observed in core 2 is likely a result of bioturbation.

Table 2 Results of the ^{210}Pb dating models

Station	CFCS model[a]			CFCS model
	Surface mixed layer[b]		mean MAR[c] (g cm^{-2} year^{-1})	^{210}Pb Flux[d] (Bq m^{-2} year^{-1})
	(cm)	(year)		
2	8	17	0.57	156
4	16	61	0.23	113
6	3	21	0.06	65
7	4	55	0.04	19
8	14	66	0.11	122
9	7	53	0.06	74
12	8	45	0.08	103
13	7	55	0.05	43
14			0.30	100

[a] Results of the CFCS model below the SML

[b] Depth (in cm) and age (estimated using the mean MAR and the mass depth) of the SML

[c] Mean mass accumulation rate beneath the SML

[d] Flux of ^{210}Pb$_{ex}$ calculated with the CF model

Numerous benthic animals were observed in this sediment core during preparation.

The SML and MAR were positively correlated ($R^2 = 0.75$; Fig. 8), indicating that sedimentation in the gulf (central and southwestern zone) is strongly associated with mixing processes. This is not surprising as the main process supplying particles to the sites (resuspension and transport by sea currents) is also mainly responsible for their mixing. This relationship may have been enhanced by the shallow water depths in the gulf. The accumulation of unconsolidated sediments (composed of carbonate and muddy skeletal sediments), in the central part of the gulf and the mainly flowing circulation in the southeast to west and southwest directions is connected with the white color observed in surficial sediments at sites 7 and 8 and with the highest MAR and SML observed at site 4 (Fig. 1). The thickness of the SML in cores 4, 7, 8, 9, 12, and 13, expressed in time units (SML in mass depth per mean MAR), ranged from 45 to 65 years. The long SML in these cores is caused the smoothing of the ^{210}Pb$_{ex}$ profile and consequently a loss of resolution in the sedimentary records.

Sediment mixing has likely smoothed the records of the anthropogenic radionuclides, especially in core 9. The slicing of the sediment cores in depth intervals of up to 5 cm is additionally responsible for part of the loss of resolution in the radionuclide profiles (Corcho-Alvarado et al. 2014). In core 9, the layer 20–25 cm is then taken as the layer of first detection of the anthropogenic radionuclides, or in other words, as the "onset of fallout" depth. Due to the large thickness of this sediment layer (5 cm) and the strong mixing of the sediments (with SML >40 years expressed in time), this assignment has a large uncertainty. In core 14, the layers containing the onset of fallout were roughly identified and their mean depths were assigned to the year 1952 (year of the onset fallout, Robbins et al. 2000). This assumption is based on the fact that Pu is strongly attached to particles and migration within the sediment cores is low in marine environment (Corcho-Alvarado et al. 2014).

In core 9, the age derived from the onset of fallout of ^{239,240}Pu (25–30 cm) shows a large disagreement with the age estimated with the CFCS ^{210}Pb model in this depth (approximately the year 1900, calculate as mass depth beneath SML/mean MAR). This disagreement may be a result of the substantial smoothing out of the ^{239,240}Pu signal by mixing in the large SML (>50 years, Table 2) and the large thickness of the layer. In core 14, on the other hand, the onset of fallout date of 1952 derived from the ^{239,240}Pu profile has a lower disagreement with the CF ^{210}Pb model age (Fig. 9). Due to the thickness of the layer, the assignment of the onset of fallout has large uncertainties. The onset of fallout could be found at any point between 25 and 30-cm depth.

The ^{210}Pb flux for each core was calculated using the ^{210}Pb$_{ex}$ inventory derived from the CF model (Table 2), according to the approach described by Sanchez-Cabeza and Ruiz-Fernández (2012). The ^{210}Pb fluxes ranged from 19 to 156 Bq m^{-2} year^{-1}, and the highest ^{210}Pb flux was found in core 2, which was collected at a site affected by high terrestrial inputs. The relatively high ^{210}Pb fluxes in cores 8 and 4 are related to high sedimentation in these areas, caused by the focusing of sediments. For site 7, located near the line of keys and a small island that divides the gulf into the west and the east sectors, the low ^{210}Pb flux may be explained by the local hydrodynamic conditions that favor resuspension and erosion (Fig. 1).

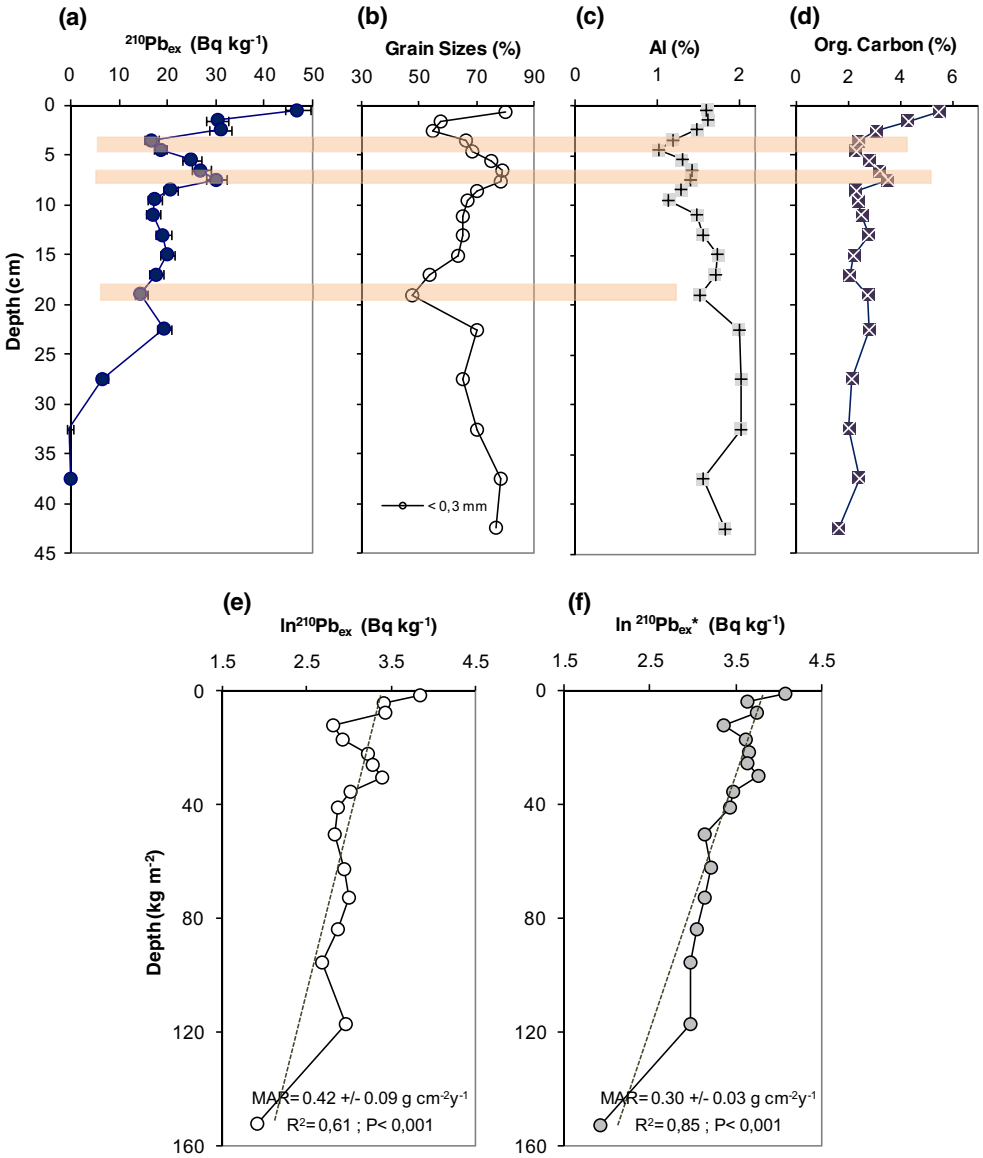

Fig. 6 Vertical profile of **a** $^{210}Pb_{ex}$, **b** grain sizes, **c** Al, and **d** organic carbon in core 14, variations were observed at the same depth. Applications of CFCS model to $^{210}Pb_{ex}$ profile without (**e**) and with Al normalization (**f**)

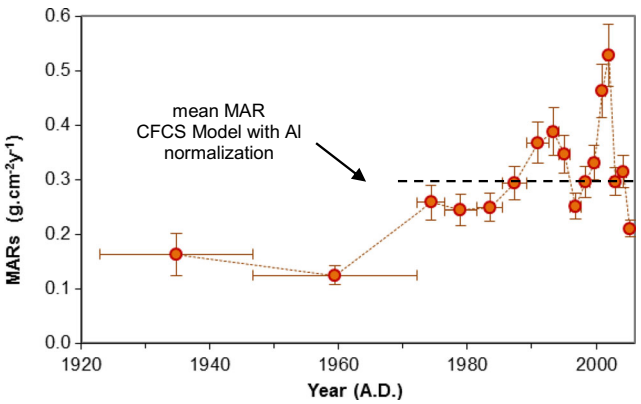

Fig. 7 Temporal evolution of the CF MARs in core 14. Mean MAR CFCS model with $^{210}Pb_{ex}$ profile with Al normalization. The MAR uncertainties and the age interval are represented

The mean $^{210}Pb_{ex}$ flux, without taking into account extreme values (lower values in sites affected by erosion and higher values in sites affected by focusing), was 77 ±25 Bq m^{-2} year^{-1}. This result is a good estimation of the atmospheric ^{210}Pb flux in the Caribbean region. The value is comparable to that reported for the Little Bahamas Bank (74–147 Bq m^{-2} year^{-1}; Henderson et al. 1999) and the Florida Bay (100–133 Bq m^{-2} year^{-1}; Robbins et al. 2000).

Total $^{239,240}Pu$ inventories were determined to be 19 Bq m^{-2} for site 9 and 27 Bq m^{-2} for site 14. The higher value in core 14 is a result of an additional input of $^{239,240}Pu$ from the mainland as this core is known to be affected by terrestrial inputs. In any case, the $^{239,240}Pu$ inventories are in good agreement with the expected $^{239,240}Pu$ inventory from global fallout in the Caribbean region (15 to 35 Bq m^{-2}; Díaz-Asencio et al. 2011; Corcho-Alvarado et al. 2014).

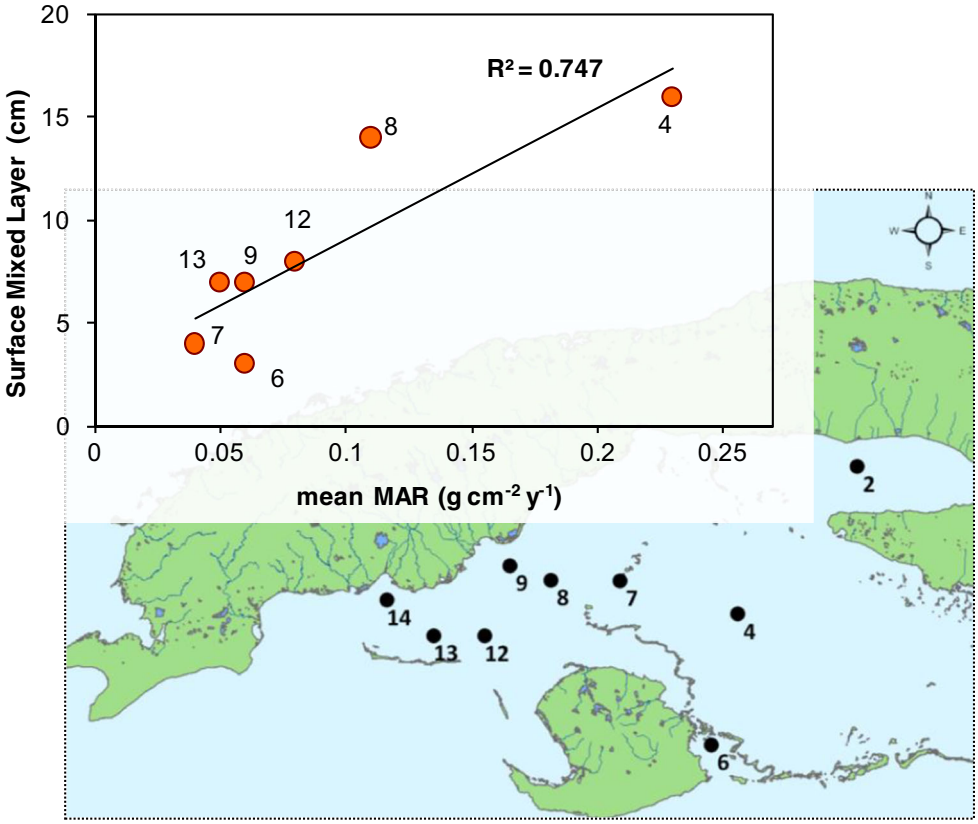

Fig. 8 **a** Linear regression of SML versus MAR in each sediment core (except core 2 and 14)

The geochemical composition of the sediments in core 7 changed significantly below 35-cm depth (Fig. 10). White carbonate-rich sediments were observed in the upper 35 cm, and dark brown colored sediments were observed below this depth. This bottom section was characterized by higher contents of organic matter (>10 %) and terrigenous elements such as Fe and Si (Fig. 10). Higher activities of ^{210}Pb and ^{226}Ra, in secular equilibrium, were also observed in the deeper part of this core (Fig. 3). Shells obtained from the sections at 37.5 and 45-cm depth showed significantly older radiocarbon ages of 1740 ± 35 and 5600 ± 45 years B.P., respectively (Fig. 10).

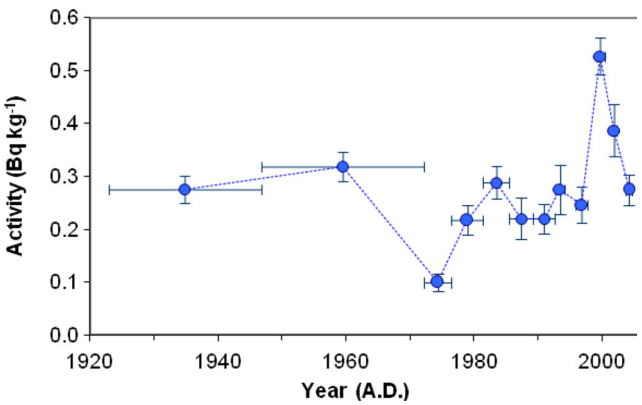

Fig. 9 Temporal evolution of the ^{239,240}Pu activity in core 14 (ages obtained with the CF model)

Assuming a constant sediment accumulation rate in the last 1740 years (along the upper 37.5 cm of this core) and not considering compaction, we estimated an apparent mean sediment accumulation rate around 0.02 cm year^{-1}. This value is of the same order of magnitude as the mean sedimentation rate calculated with the CFCS ^{210}Pb model (0.09 ± 0.01 cm year^{-1}).

Ionin et al. (1977) reported the occurrence of organic-rich layers in the deepest part of several sediment cores from the Batabano Gulf. The origin of such layers (with mangrove rest) was linked to the ancient coastal line. These results suggest that the bottom part of the core 7 (below 35 cm) might be an ancient intertidal coastal zone that is currently submerged due to the relative sea level rise during the Holocene (Scholl et al. 1969; Enos and Perkins 1979; Davies and Cohen 1989).

Sedimentation Processes in the Gulf of Batabano

Our results revealed the existence of three sedimentary environments in the study region. Due to the shallow depth, sea currents and winds (stronger during storms) cause turbulence and resuspension of recent sediments, preferentially in the fine fraction. These conditions were clearly observed in the central part of the Gulf of Batabano, where core 4 was characterized by a large SML (16 cm) and a highly smoothed environmental record. The sediment core may nonetheless be used as

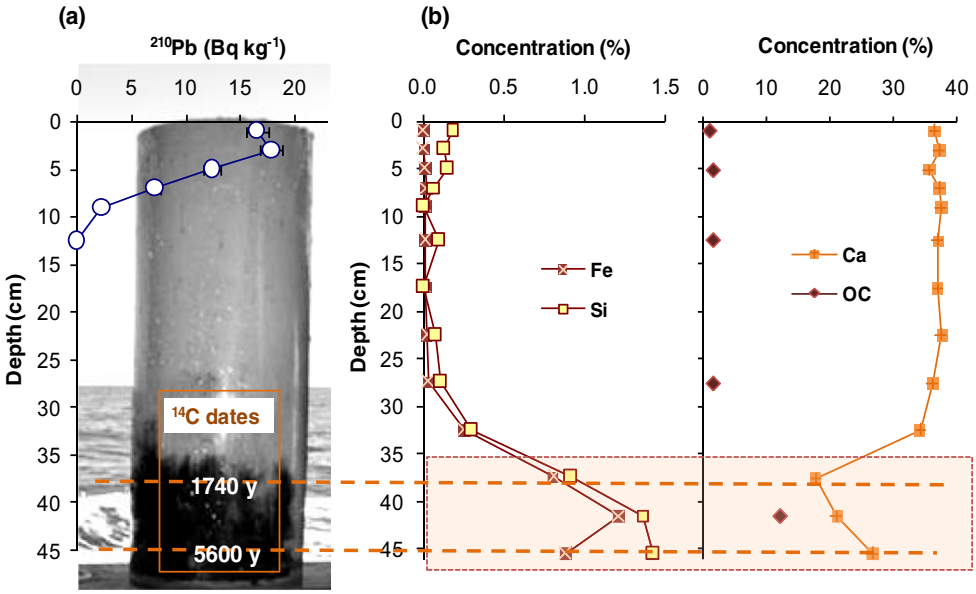

Fig. 10 **a** Radiocarbon ages (B.P.) of shells in sediment and vertical profile of $^{210}Pb_{ex}$ in core 7. The sediment core shows a strong color change at the bottom part of the core. **b** Fe, Si, Ca, and organic carbon concentration profiles in core 7

environmental archive of older proxy data. In this part of the gulf, the sediments contain large amounts of carbonates produced in the southeastern areas (Avello Suarez and Pavlidis 1986). Site 7, which is also located in the central part of the Gulf but with local hydrodynamic conditions, was characterized by a low MAR (0.04 ± 0.01 g cm^{-2} year^{-1}) and a relatively thin SML (4 cm).

A second sedimentary environment was identified in the southwestern part of the gulf (sites 9, 12, and 13). This zone is separated from the first zone by a line of cays and small

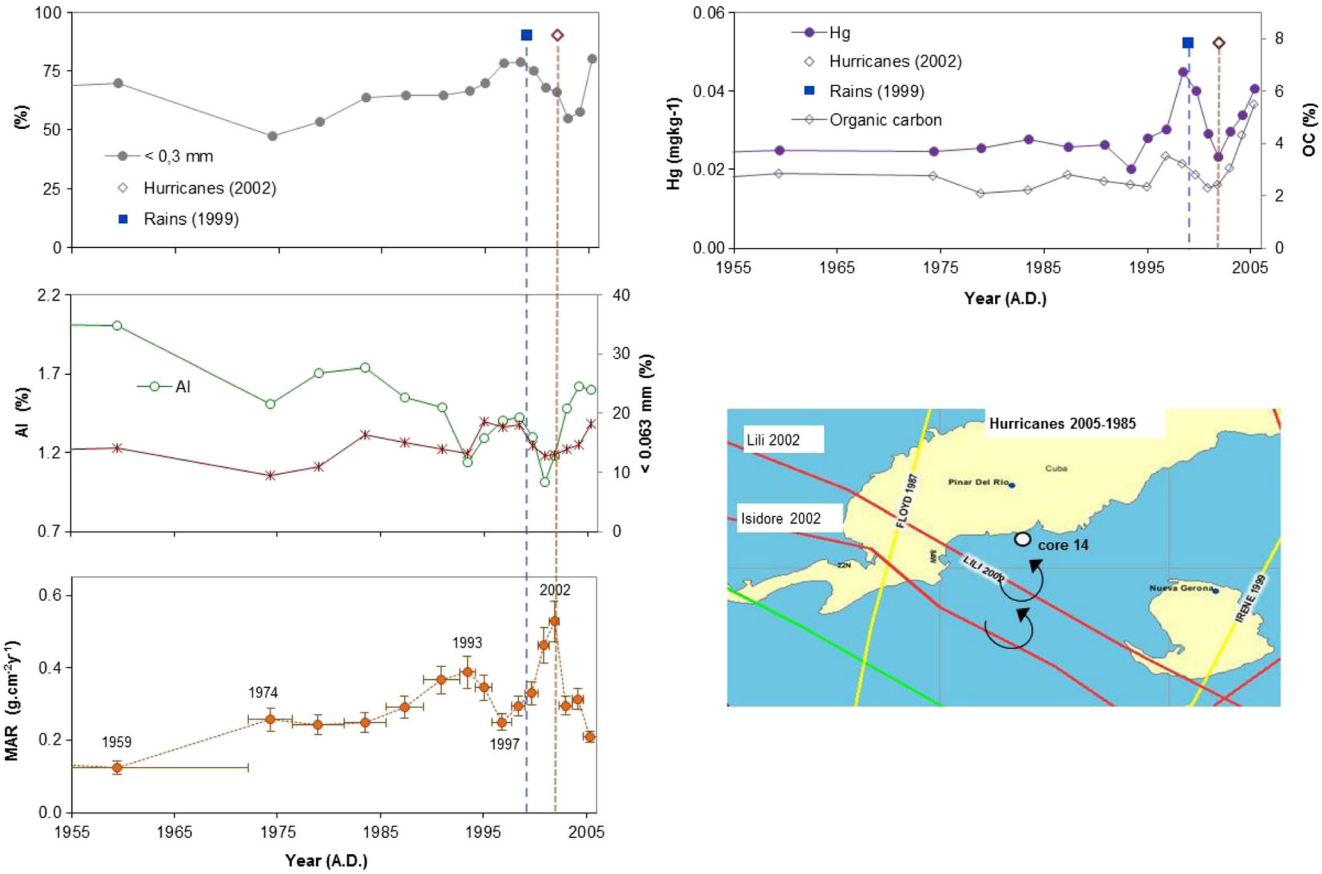

Fig. 11 Temporal variation of the grain size (<0.3 mm), mercury, organic carbon, aluminum, and MARs in core 14. Variations of these parameters were observed after the intensive rains of 1999 and the hurricanes of 2002

islands and is influenced more by terrigenous inputs. The cores from this region showed lower MARs (0.05 to 0.08 g cm^{-}2 year^{-1}) and thinner SMLs (7–8 cm) in comparison to the first sedimentary zone. Nonetheless, the long mixing times in the SMLs of 45–55 years have smoothed out the sedimentary records. Core 8 shows results that indicate it to be located in a transition zone between both sedimentary environments.

A third sedimentary environment corresponds to the sites located close to the coastline (sites 2 and 14), which are characterized by the highest MARs (0.57 to 0.30 g cm^{-2} year^{-1}). The CF MARs in site 14 showed increasing values after 1970 with two peaks around 1993 and 2002. In this core, recent variability is also observed in the irregular distributions of Hg, Al, organic carbon, and grain size (Fig. 11; Armenteros et al. 2011). The Al decrease after the 1970s is likely linked to reduced terrigenous input due to changes in land use and due to the construction of dams and dikes reported in the catchment area of the gulf (Alonso et al. 2011). The lower values in Al after 1980 are mostly related to low amounts of fine particles. After 1990, organic carbon and Hg showed significant variations and similar patterns, with a peak around 1999 and lower values in 2002. These results suggest that organic matter might be an efficient carrier of trace earth elements, such as Hg (Sanders et al. 2006). Moreover, the peak observed in 1999 is possibly connected with terrestrial runoff (Fig. 11).

Sedimentary and geochemical records in the sediment cores are related with some extreme climatic events reported in the gulf. The intensive rains reported in La Coloma in 1999 are known to have induced extensive soil erosion in the catchment's basin and consequently an increased input of terrestrial Al, organic carbon, Hg, and the radionuclides ^{239,240}Pu into the gulf. The hurricanes Lili and Isodore that affected the Cuban region in 2012 mainly caused the transport of large amounts of suspended matter in sea water in the northeastern direction. The suspended matter of marine origin and therefore poor in terrigenous elements caused the dilution of the terrigenous runoff. This process may explain the minimum levels of the terrestrial indicators observed in 2002 and the maximum MAR calculated for this date (Fig. 11).These additional evidences further corroborate the core radiochronology.

Conclusions

Radiometrically dated sediment cores enabled us to quantify sedimentation and mixing processes over the past 100 years in the Gulf of Batabano. The CFCS and CF models were applied to interpret the ^{210}Pb data in the segments below the mixed layers. Both models provided valuable information about sedimentary processes in this highly dynamic ecosystem. The shallow water depths in the study region, combined with the frequent storms in the area, have caused physical mixing of surface sediments. We identified three main sedimentary zones: the first located in the central part of the gulf with large MAR and intense mixing processes, the second located in the southwestern region with lower MAR and mixing in comparison to the first, and the third zone located close to the coastline which has the highest MARs and lower mixing. Surface mixed layers were observed in most regions of the gulf, which has affected the time resolution of most sedimentary records. Extreme climatic events, such as intense rains and hurricanes, caused changes in the mass accumulation rates and sediment composition. The data provided evidence that part of the present Gulf of Batabano was an ancient intertidal coastal zone that is currently submerged due to the relative sea level rise from 5600 to 1740 year B.P.

Acknowledgments This work was supported by the IAEA Technical Cooperation Project CUB7/006. We also acknowledge the Swiss Federal Office for Public Health (OFSP) and the CONACYT (project CB-2010/153492, Mexico) for some financial support. We acknowledge support for radiocarbon analyses from the National Science Foundation (Cooperative Agreement number, OCE-9807266). This work has involved a large number of people, and it is impossible to list all of them here. We would like to thank the sampling team: Miguel Gómez (from CEAC); Yanis Cruz, Alexander Lopeztegui, and Rafael Fuentes (from Centro de Investigaciones Pesqueras, Havana, Cuba); to the ALECRIN II tripulation: Reinaldo Hernandez (Captain), Tomas Serrano, and Ceferino Lara; and special thanks to Norberto Capetillo and Julio Baisre. We would like to give special thanks to Aniel Guillen from CEAC and Jean Bartocci (from IAEA-MEL), Laval Liong Wee Kwong, Janine Gastaud (in memoriam) from the Radiometrics Laboratory of the IAEA Environment Laboratories. We are also grateful to IAEA Technical Cooperation Department and the Project Managers Michel Warnau and Carlos Alonso. We also give special thanks to Carlo Papucci and Roberta Delfanti for the detailed review of results and J.M. Smoak for the review of the manuscript.

References

Alonso-Hernández, C.M., F. Conte, C. Misic, M. Barsanti, M. Gómez-Batista, M. Díaz-Asencio, A. Covazzi-Harriague, and F.G. Pannacciulli. 2011. An overview of the Gulf of Batabanó (Cuba): environmental features as revealed by surface sediment characterisation. *Continental Shelf Research* 31: 749–757.

Appleby, P.G., and F. Olfield. 1978. The calculation of lead-210 dates assuming a constant rate of supply of unsupported ^{210}Pb to the sediment. *CATENA* 5: 1–8.

Armenteros, M., M. Díaz-Asencio, R. Fernández-Garcés, M. Eriksson, C. Alonso-Hernández, and J.A. Sanchez-Cabeza. 2011. Historical changes of sediments and mollusk assemblages in the Gulf of Batabanó (Caribbean Sea) in the twentieth century. *Environmental Monitoring and Assessment* 184: 4709–4723.

Avello Suarez, O., Pavlidis, Y.A. 1986. Sedimentos de la plataforma cubana. III. Golfo de Batabanó. Instituto de Geología y Paleontología. Academia de Ciencia de Cuba. Reporte de Investigación 6, pp. 42.

Baisre, J. 2010. Setting a baseline for Caribbean fisheries. *Journal of Island & Coastal Archaeology* 5: 120–147.

Baskaran, M., and A. Naidu. 1995. ^{210}Pb-derived chronology and the fluxes of ^{210}Pb and ^{137}Cs isotopes into continental shelf sediments,

East Chukchi Sea, Alaskan Arctic. *Geochimica et Cosmochimica Acta* 59: 4435–4448.

Boer, W., G.D. van den Bergh, H. de Haas, H.C. de Stigter, R. Gieles, and C.E. van Weering. 2006. Validation of accumulation rates in Teluk Banten (Indonesia) from commonly applied ^{210}Pb models, using the 1883 Krakatau tephra as time marker. *Marine Geology* 227: 263–277.

Caddy, J.F., and D.J. Agnew. 2004. An overview of recent global experience with recovery plans for depleted marine resources and suggested guidelines for recovery planning. *Reviews in Fish Biology and Fisheries* 14: 43–112.

Carpenter, R., M.L. Peterson, and J.T. Bennett. 1982. ^{210}Pb-derived sediment accumulation and mixing rates for the Washington continental slope. *Marine Geology* 48: 135–164.

Cerdeira-Estrada, S., S. Lorenzo-Sánchez, A. Areces-Mallea, and C. Martínez-Bayón. 2008. Mapping of the spatial distribution of benthic habitats in the Gulf of Batabanó using Landsat-7 images. *Ciencias Marinas* 34: 213–222.

Claro, R., Y. Sadovy de Mitcheson, K.C. Lindeman, and A.R. García-Cagide. 2009. Historical analysis of Cuban commercial fishing effort and the effects of management interventions on important reef fishes from 1960–2005. *Fisheries Research* 99: 7–16.

Corcho-Alvarado, J.A., M. Díaz-Asencio, P. Froidevaux, F. Bochud, C.M. Alonso-Hernández, and J.A. Sanchez-Cabeza. 2014. Dating young Holocene coastal sediments in tropical regions: use of fallout ^{239,240}Pu as alternative chronostratigraphic marker. *Quaternary Geochronology* 22: 1–10.

Cruz, R., E. Díaz, M. Báez, and R. Adriano. 2001. Variability in recruitment of multiple life stages of the Caribbean spiny lobster, Panulirus argus, in the Gulf of Batabanó, Cuba. *Marine and Freshwater Research* 52: 1263–1270.

Davies, T.D., and A.D. Cohen. 1989. Composition and significance of the peat deposits of Florida Bay. *Bulletin of Marine Science* 44: 387–398.

Díaz-Asencio, M., C.M. Alonso-Hernández, Y. Bolaños-Álvarez, M. Gómez-Batista, V. Pinto, R. Morabito, J.I. Hernández-Albernas, M. Eriksson, and J.A. Sanchez-Cabeza. 2009. One century sedimentary record of Hg and Pb pollution in the Sagua estuary (Cuba) derived from ^{210}Pb and ^{137}Cs chronology. *Marine Pollution Bulletin* 59: 108–115.

Díaz-Asencio, M., J.A. Corcho-Alvarado, C. Alonso-Hernández, A. Quejido-Cabezas, A.C. Ruiz-Fernández, M. Sanchez-Sanchez, M.B. Gómez-Mancebo, P. Froidevaux, and J.A. Sanchez-Cabeza. 2011. Reconstruction of metal pollution and recent sedimentation processes in Havana Bay (Cuba): a tool for coastal ecosystem management. *Journal of Hazardous Materials* 196: 402–411.

Enos, P., and R.D. Perkins. 1979. Evolution of Florida Bay from island stratigraphy. *Bulletin Geological Society of America* 90: 59–83.

González-Yáñez, A.A., R. Puga Millán, M. Estela.de León, L. Cruz-Font, and M. Wolff. 2006. Modified Delury depletion model applied to spiny lobster, Panulirus argus (Latreille, 1804) stock, in the southwest of the Cuban Shelf. *Fisheries Research* 79: 155–161.

Henderson, G.M., F.N. Lindsay, and N.C. Slowey. 1999. Variation in bioturbation with water depth on marine slopes: a study on the Little Bahamas Bank. *Marine Geology* 160: 105–118.

Hernández González, M., and G. Díaz Llanes. 2003. Some considerations on the variability of sea level synoptic component in the Gulf of Batabanó. *Serie Oceanológica* 1: 10–24.

Hoskins, C.W. 1964. Molluscan biofacies in calcareous sediments, Gulf of Batabano, Cuba. *American Association of Petroleum Geologists Bulletin* 48: 1680–1704.

Ionin, A.S., Y.A. Pavlidis, and O.S. Avello. 1977. *Geología de la Plataforma Marina de Cuba*. Moscú: Editorial Nauka.

Lewis, R.C., K.H. Coale, B.D. Edwards, M. Marot, J.N. Douglas, and E.J. Burton. 2002. Accumulation rate and mixing of shelf sediments in the Monterey Bay National Marine Sanctuary. *Marine Geology* 181: 157–169.

Luisier, F., J.A. Corcho Alvarado, P. Steinmann, M. Krachler, and P. Froidevaux. 2009. A new method for the determination of plutonium and americium, using high pressure microwave digestion and alpha-spectrometry or ICP-SMS. *Journal of Radioanalytical and Nuclear Chemistry* 281: 425–432.

Nittrouer, C.A., D.J. DeMaster, B.A. Mckee, and N.H. Cutshall. 1984. The effect of sediment mixing on ^{210}Pb accumulation rates for the Washington continental shelf. *Marine Geology* 54: 201–221.

Oldfield, F., Appleby, P.G. 1984. Empirical testing of ^{210}Pb dating models for lake sediments. In Lake sediments and environmental history, eds. E.Y. Haworth, W. Lund, 93–124. Leicester University Press.

Puga, R., M.E. De Leon, and R. Cruz. 1996. Catchability for the main fishing methods in the Cuban fishery of the spiny lobster Panulirus argus (Latreille, 1804), and implications for management (Decapoda, Palinuridea). *Crustaceana* 69: 703–718.

Puga, R., S. Hernández Vázquez, J. López Martinez, and M.E. de León. 2005. Bioeconomic modelling and risk assessment of the Cuban fishery for spiny lobster Panulirus argus. *Fisheries Research* 75: 149–163.

Reimer, P.J., M.G.L. Baillie, E. Bard, A. Bayliss, J.W. Beck, P.G. Blackwell, C. Bronk Ramsey, C.E. Buck, G.S. Burr, R.L. Edwards, M. Friedrich, P.M. Grootes, T.P. Guilderson, I. Hajdas, T.J. Heaton, A.G. Hogg, K.A. Hughen, K.F. Kaiser, B. Kromer, G. McCormac, S.W. Manning, R.W. Reimer, D.A. Richards, J.R. Southon, S. Talamo, C.S.M. Turney, J. van der Plicht, and C.E. Weyhenmeyer. 2009. IntCal09 and Marine09 radiocarbon age calibration curves, 0–50,000 years cal BP. *Radiocarbon* 51: 1111–1150.

Robbins, J.A., and D.N. Edgington. 1975. Determination of recent sedimentation rates in Lake Michigan Using Pb-210 and Cs-137. *Geochimical et Cosmochimica Acta* 39: 285–304.

Robbins, J.A., C. Holmes, R. Halley, M. Bothner, E. Shinn, J. Graney, G. Keeler, M. TenBrink, K.A. Orlandini, and D. Rudnick. 2000. Time-averaged fluxes of lead and fallout radionuclides to sediments in Florida Bay. *Journal of Geophysical Research* 105: 28 805–28 821.

Rude, P.D., and R.C. Aller. 1991. Fluorine mobility during early diagenesis of carbonate sediment: an indicator of mineral transformation. *Geochimica et Cosmochimica Acta* 55: 2491–2509.

Ruiz-Fernández, A.C., M. Frignani, C. Hillaire-Marcel, B. Ghaleb, M.D. Arvizu, J.R. Raygoza-Viera, and F. Páez-Osuna. 2009. Trace metals (Cd, Cu, Hg, and Pb) accumulation recorded in the intertidal mudflat sediments of three coastal lagoons in the Gulf of California, Mexico. *Estuaries and Coasts* 32: 551–564.

Sanchez-Cabeza, J.A., Masqué, P., Ani-Ragolta, I. 1998.^{210}Pb and ^{210}Po analysis in sediments and soils by microwave acid digestion. Journal of Radioanalytical and Nuclear Chemistry 227, 19–22.

Sanchez-Cabeza, J.A., P. Masque, I. Ani-Ragolta, J. Merino, M. Frignani, F. Alvisi, A. Palanques, and P. Puig. 1999. Sediment accumulation rates in the southern Barcelona continental margin (NW Mediterranean Sea) derived from ^{210}Pb and ^{137}Cs chronology. *Progress in Oceanography* 44: 313–332.

Sanchez-Cabeza, J.A., and A.C. Ruiz-Fernández. 2012. ^{210}Pb sediment radiochronology: an integrated formulation and classification of dating models. *Geochimica et Cosmochimica Acta* 82: 183–200.

Sanders, C.J., I.R. Santos, E.V. Silva-Filho, and S.R. Patchineelam. 2006. Mercury flux to estuarine sediments, derived from Pb-210 and Cs-137 geochronologies (Guaratuba Bay, Brazil). *Marine Pollution Bulletin* 52: 1085–1089.

Sanders, C.J., P.P. Caldeira, J.M. Smoak, M.E. Ketterer, A. Belem, U.M.N. Mendoza, L.G.M.S. Cordeiro, E.V. Silva-Filho, S.R. Patchineelam, and A.L.S. Albuquerque. 2014. Recent organic carbon accumulation (~100 years) along the Cabo Frio, Brazil upwelling region. *Continental Shelf Research* 75: 68–75.

Santschi, P.H., L. Guo, S. Asbill, M. Allison, A. Britt Kepple, and L. Wen. 2001. Accumulation rates and sources of sediments and organic carbon on the Palos Verdes shelf based on radioisotopic tracers (^{137}Cs, ^{239,240}Pu, ^{210}Pb, ^{234}Th, ^{238}U and ^{14}C). *Marine Chemistry* 73: 125–152.

Scholl, D.W., F.W. Craighead Sr., and M. Stuiver. 1969. Florida submergence curve revised: Its relation to sedimentation rates. *Science* 163: 562–564.

Smoak, J.M. 2015. Sediment mixing rate, ^{210}Pb and ^{234}Th. *In Encyclopedia of Scientific Dating Methods*, eds. W.J. Rink, J. Thompson. Berlin, Springer-Verlag.